journal

J. Am. Ceram. Soc., 77 [10] 2518–22 (1994)

Toughness Properties of a Silicon Carbide with an *in Situ* Induced Heterogeneous Grain Structure

Nitin P. Padture*,† and Brian R. Lawn*

Materials Science and Engineering Laboratory, National Institute of Standards and Technology, Gaithersburg, Maryland 20899

Toughness characteristics of a heterogeneous silicon carbide with a coarsened and elongated grain structure and an intergranular second phase are evaluated relative to a homogeneous, fine-grain control using indentation–strength data. The heterogeneous material exhibits a distinctive flaw tolerance, indicative of a pronounced toughness curve. Quantitative evaluation of the data reveals an enhanced toughness in the long-crack region, with the implication of degraded toughness in the short-crack region. The enhanced long-crack toughness is identified with crack-interface bridging. The degraded short-crack toughness is attributed to weakened grain or interface boundaries and to internal residual stresses from thermal expansion mismatch. A profound manifestation of the toughness-curve behavior is a transition in the nature of mechanical damage in Hertzian contacts, from classical single-crack cone fracture in the homogeneous control to distributed subsurface damage in the heterogeneous material.

I. Introduction

In a previous paper, a new *in situ* processing strategy for tailoring dense silicon carbide (SiC) ceramics with heterogeneous microstructures was reported.[1] Using yttria and alumina sintering agents, a coarse and elongate microstructure was obtained, with a residual intergranular second phase. In contrast to a homogeneous fine-grain control SiC material, the fracture was found to be highly intergranular with copious crack-interface bridging, indicating weak and highly stressed interphase boundaries. Preliminary measurements of Vickers indent crack dimensions indicated more than a twofold increase in the long-crack toughness.

Such heterogeneous microstructural features have been identified as principal elements of effective grain bridging, and thence of toughness-curve (*R*- or *T*-curve) behavior, in monophase and two-phase ceramics.[2–10] To this end, *in situ* processing of materials with elongate-shaped reinforcements, used first in the fabrication of glass-ceramics[11,12] and more recently of silicon nitrides,[13,14] offers several advantages: avoidance of health hazards associated with conventional whisker reinforcement; potentially high volume fractions of reinforcement phase; fabrication of low-cost, complex, large components; and atmospheric-pressure processing. Significant improvements in long-crack toughness, and attendant flaw tolerance, have been previously realized by this route.[13–15] However, the same heterogeneous features can diminish the short-crack toughness, by providing easy fracture paths at large grain facets in residual tension.[6,9,10,16] As a consequence, laboratory strength[17] and wear resistance[18,19] can be degraded. Effective materials design for specific structural applications therefore involves due compromise between countervailing short- and long-crack properties.

Accordingly, in this paper we present results of a detailed investigation of the long- and short-crack toughness properties of our heterogeneous SiC ceramic, in relation to a homogeneous fine-grain control. Indentation–strength tests are used to determine the flaw tolerance[20,21] and toughness-curve[22] characteristics. The strength and toughness are shown to be enhanced in the long-crack region by crack-interface bridging from interlocking grains. Conversely, these same properties are diminished in the short-crack region by weak interphase boundaries and internal residual stresses. The latter microstructural features are responsible for a fundamental transition in the local stress–strain response at Hertzian contacts, from "elastic–brittle" in the homogeneous control to "elastic–ductile" in the heterogeneous material.

II. Experimental Procedure

Specimens of heterogeneous SiC were prepared by *in situ* processing, as previously described.[1] Starting powders of β-SiC with 0.5 vol% α-SiC for seeding were liquid-phase pressureless sintered with the aid of yttria and alumina additives at 1900°C for 0.5 h. A second heat treatment at 2000°C for 3 h was then used to effect a complete β–α transition in the SiC, and thereby cause grain growth.The final microstructure had elongated SiC grains ≈3 μm thick by ≈25 μm long, with 20 vol% yttrium aluminum garnet (YAG) crystalline intergranular phase, and was 97% dense. The difference in thermal expansion coefficient between SiC and YAG is $\approx 5 \times 10^{-6}\ °C^{-1}$, leading to substantial residual stresses at the interphase boundaries.[1]

Specimens were also prepared from a relatively homogeneous, commercial pressureless sintered SiC material (Hexoloy SA, Carborundum, Niagara Falls, NY), to establish a reference baseline for the ensuing test results. This material had an equiaxed, well-bonded microstructure of mean grain size ≈4 μm, again with density 97%.

Disks 20-mm diameter and 2.5-mm thickness were ground from the bulk SiC and diamond-polished to 1-μm finish. Most of these specimens were indented in air at the center of the polished face with a Vickers diamond pyramid, at contact loads from $P = 1$ to 300 N. Surfaces of a select few indented specimens with indentation cracks were sputter-coated with gold and viewed in a scanning electron microscope. Some disks were left without Vickers indentations, for measurement of "laboratory" strengths and for Hertzian contact experiments.

The bulk of the disks were broken in biaxial flexure with the polished sides in tension, using a three-point support and circular-flat loading fixture[23] on a universal testing machine (Model 1122, Instron, Canton, MA). To avoid environmental effects, a drop of moisture-free silicone oil was placed on each polished surface immediately prior to flexure, and the disk broken in rapid loading (failure time <10 ms). Strengths σ_F were calculated from the failure loads and specimen dimensions.[23] Care

G. Grathwohl—contributing editor

Manuscript No. 194010. Received December 14, 1993; approved June 17, 1994.
Supported by the U.S. Air Force Office of Scientific Research.
*Member, American Ceramic Society.
†Guest Scientist, on leave from Department of Materials Science and Engineering, Lehigh University, Bethlehem, PA 18015.

was taken to examine all broken disks to ensure that failures originated from the indentations. Those disks that did not fail from an indentation site were included in the laboratory strength data pool for unindented specimens.

Hertzian contact tests were carried out using tungsten carbide spheres of radius $r = 1.58$ to 12.7 mm.[24,25] For prescribed values of P and r, contact radii a were measured from impressions left in metal coatings on the polished surfaces. These measurements enabled plots of indentation pressure $p_0 = P/\pi a^2$ vs indentation strain a/r to be constructed.[24] A special specimen configuration, consisting of two polished rectangular half-blocks bonded together with thin adhesive, was used to obtain section as well as surface views of the contact damage.[25] Indentations were made symmetrically across the surface trace of the bonded interface on the top surface. The adhesive was then dissolved and the half-blocks separated. Finally, the top and side surfaces were gold-coated, and viewed in optical Nomarski illumination and scanning electron microscope (SEM) imaging to reveal the damage pattern.

III. Results

(1) Observations of Crack-Interface Bridging

Observations were made of radial cracks at Vickers indentations in the SEM to determine the fracture morphology of the SiC. Examples are shown in Figs. 1 and 2. Figures 1(A) and (B) compare crack paths in the homogeneous control SiC and the heterogeneous test material, respectively. In the homogeneous SiC, the crack is relatively straight and transgranular, with no indication of crack-wake bridging. By contrast, the crack in the heterogeneous material follows a deflected path along interphase boundaries, and bridging sites are most apparent.

Figures 2(A) and (B) show examples of crack-wake bridging sites in the heterogeneous SiC. These micrographs highlight the debonding along the relatively weak interphase boundaries. Secondary fractures adjacent to the separating surfaces are evident, reflecting the action of considerable frictional tractions during grain pullout.[3]

(2) Indentation–Strength and Toughness Curves

Figure 3 shows the indentation–strength $\sigma_F(P)$, response of the heterogeneous SiC, along with comparative data for the homogeneous fine-grain control material. In the heterogeneous material, the radial crack patterns were well formed at all indentation loads. In the homogeneous material, however, the patterns showed severe chipping at loads $P > 30$ N, from lateral cracks. Such chipping has been shown to lead to artificially high strength values, by relieving the residual stress field around the Vickers indentations.[26] With this allowance, the remainder of the homogeneous SiC data follow a classical $\sigma_F \propto P^{-1/3}$ response (dashed line) for materials with single-valued toughness.[27] Relative to this baseline, we see that the heterogeneous material (solid curve) exhibits pronounced flaw tolerance, with strongly enhanced long-crack strength. At low loads, the curve for the heterogeneous material appears on the verge of crossing the homogeneous data line, suggesting degraded short-crack strength properties. Such a crossover is consistent with the reduced laboratory strength for the heterogeneous material in Fig. 3.

Toughness curves $T(c)$ may be deconvoluted directly from the data in Fig. 3 in accordance with an indentation–strength K-field analysis.[28,29] Under the action of an applied stress σ_A, radial cracks of size c produced at indentation load P extend according to the equilibrium condition

$$K'_A(c) = \psi\sigma_A c^{1/2} + \chi P/c^{3/2} = T(c) \qquad (1)$$

where $K'_A(c)$ is a "global" applied stress-intensity factor, and ψ

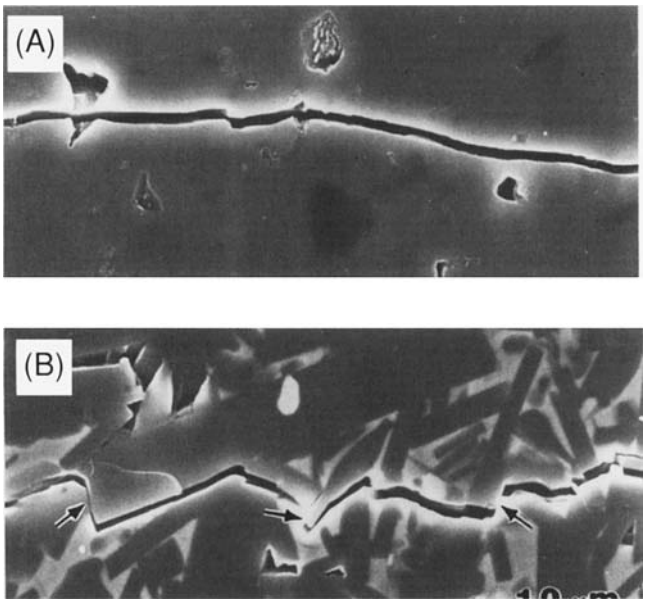

Fig. 1. SEM views of cracks in (A) homogeneous control and (B) heterogeneous test SiC. Note relatively straight, transgranular path in (A), and bridged, intergranular path in (B). (After Ref. 1.)

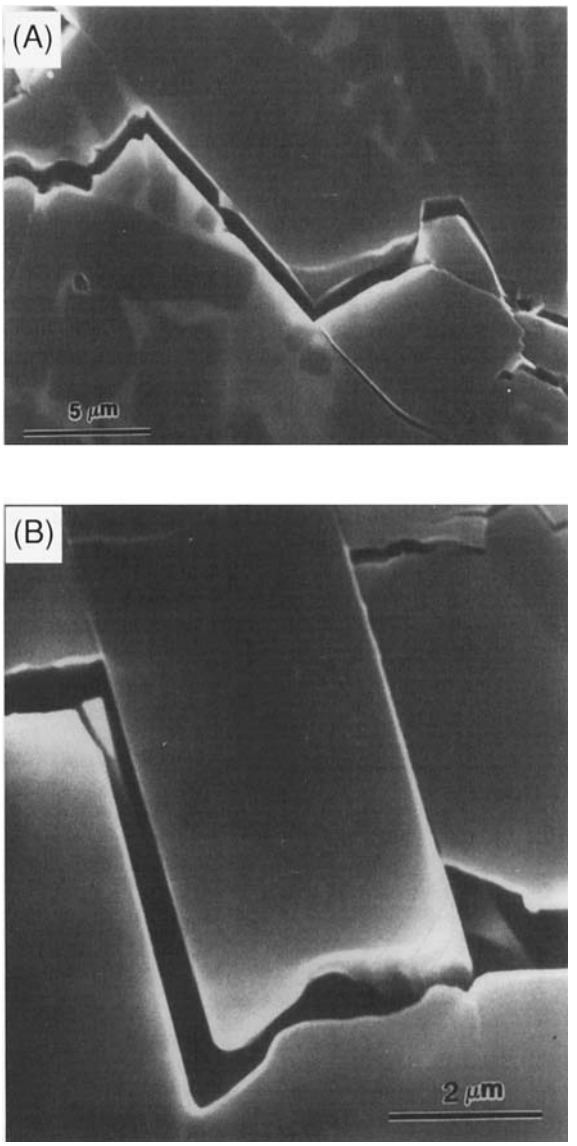

Fig. 2. SEM views of crack-wake bridging by elongate SiC grains in heterogeneous SiC. Note secondary microfractures at pullout grains.

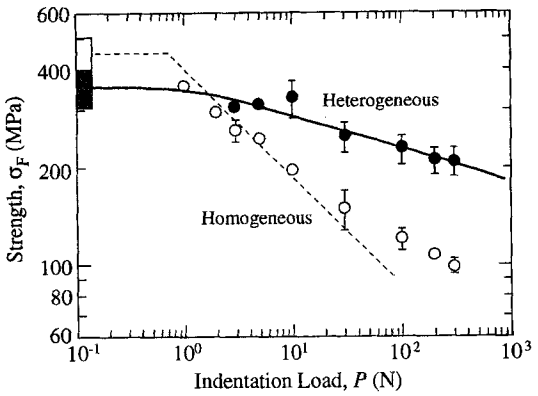

Fig. 3. Indentation–strength data for heterogeneous test and homogeneous control SiC. For heterogeneous material, each point with standard deviation bar represents average of breaks from three to five specimens. Boxes at left axis are "laboratory" strengths, representing breaks from unindented specimens.

and χ are crack-geometry and residual-contact coefficients. For a given load P, failure occurs at that applied stress $\sigma_A = \sigma_F$ which satisfies the "tangency condition"

$$dK'_A(c)/dc = dT(c)/dc. \quad (2)$$

Accordingly, given an appropriate calibration of the coefficients ψ and χ, we may generate families of $K'_A(c)$ curves from the $\sigma_F(P)$ data sets in Fig. 3. Toughness curves $T(c)$ may then be objectively determined as envelopes to these families of curves.[22]

Such constructions are made in Figs. 4(A) and (B) for the homogeneous and heterogeneous SiC ceramics, respectively, as follows:[22]

(i) For the homogeneous control material, satisfaction of the condition $\sigma_F \propto P^{-1/3}$ in Fig. 3 implies a single-valued toughness, $T(c) = T_0 =$ constant. A previous study on alumina[22] makes use of this condition in a fine-grain control to calibrate ψ and χ in Eq. (1). Assuming the Vickers crack geometry to be material-independent, we may retain $\psi = 0.77$ from that previous study.[22] Allowing for a dependence in the residual contact field on the modulus-to-hardness ratio $(E/H)^{1/2} = (410\text{ GPa}/24.8\text{ GPa})^{1/2} = 16.5$,[30] we obtain $\chi = 0.067$ for SiC-based ceramics from that same previous study. The best-fit line through the control data set in Fig. 3 corresponds to the solution of Eqs. (1) and (2) at $T(c) = T_0 = 2.1$ MPa·m$^{1/2}$. A family of $K'_A(c)$ curves can now be generated from the control indentation–strength data (Fig. 4(A)), inserting $\sigma_A = \sigma_F$ at each value of P in Eq. (1). We see that the envelope of tangency points is approximately horizontal in this case, validating the calibration and confirming a single-valued toughness for this material.

(ii) For the heterogeneous test material, we use the same values of ψ and χ,[1,‡] and generate another family of $K'_A(c)$ curves from the indentation–strength data in Fig. 4(B). The envelope of tangency points now yields a rising $T(c)$ curve. In the long-crack region ($c >> 100$ μm), the toughness increases relative to the control value, by a factor of about three. It might be presumed, by data extrapolation, that the toughness similarly *decreases* in the short-crack region ($c << 100$ μm).[22] However, rather than relying on such an extrapolation here, we demonstrate the short-crack degradation with the following Hertzian contact results.

(3) Hertzian Contact and Subsurface Deformation

Hertzian contact tests were conducted on both the homogeneous control and heterogeneous test SiC materials. Figure 5 shows half-surface and section views of the ensuing contact damage, at sphere radius $r = 3.18$ mm and load $P = 2000$ N. In the homogeneous control SiC (Fig. 5(A)), we observe the familiar cone crack pattern *outside* the contact circle.[31] The crack path is transgranular and uninterrupted (cf. Fig. 1(A)). On the other hand, in the heterogeneous SiC (Fig. 5(B)), we observe a subsurface zone of distributed damage *beneath* the contact circle, strikingly reminiscent of the plastic zones that typify contacts in metals.[32,33] Figure 6, a higher magnification view of this latter damage zone, reveals a network of facet-length debonding failures along the weak interphase boundaries.

Figure 7 plots indentation stress–strain curves for the two SiC forms. The dashed line represents the Hertzian relation for perfectly elastic contacts[34,35] on the homogeneous control:

$$p_0 = (3E/4\pi k)(a/r) \quad (3)$$

with $E = 410$ GPa Young's modulus (SiC) and $k = 0.90$ (tungsten carbide on SiC). The curve for the homogeneous SiC lies close to the elastic ideal over the data range, notwithstanding the incidence of cone fracture and possible inelastic deformation of the tungsten carbide sphere.[24] By contrast, the curve for the heterogeneous SiC deviates markedly from the dashed line ideal above a critical pressure $p_0 \approx 5$ GPa, indicating the onset of "yield." This latter critical pressure corresponds to that at which subsurface damage of the kind shown in Fig. 5(B) first becomes detectable.

‡Whereas, for the homogeneous control, we have $E/H = 16.5$, for the heterogeneous test material with YAG second phase we have $E/H = 17.2$.[1] This corresponds to a difference of <2% in $(E/H)^{1/2}$, which is considered insignificantly small in relation to the constructions of Fig. 4.

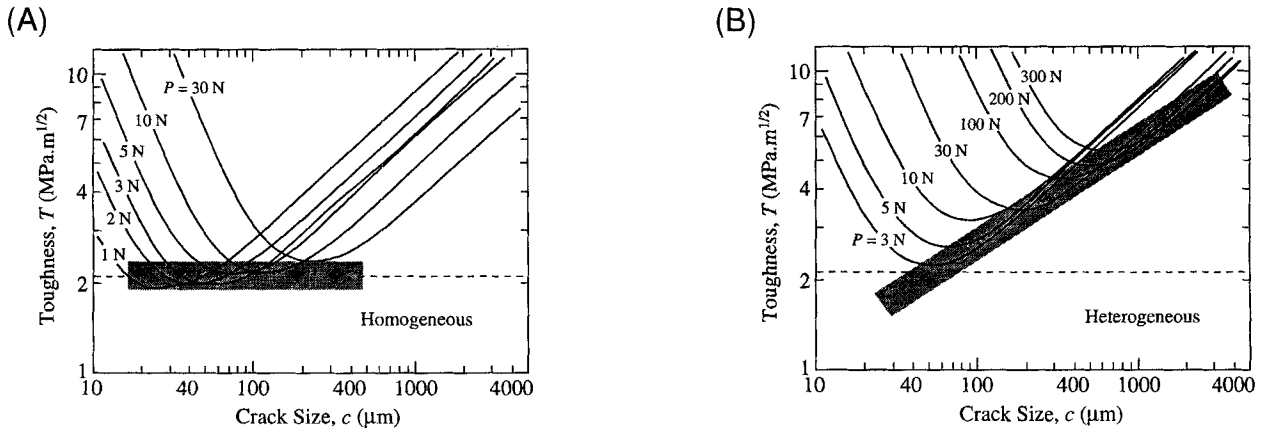

Fig. 4. Toughness-curve diagrams for (A) homogeneous control and (B) heterogeneous test SiC. Family of solid curves are plots of $K'_A(c)$ in Eq. (1), using strength data from Fig. 3. Shaded bands are T-curves, plotted as locus of tangency points to $K'_A(c)$ curves.

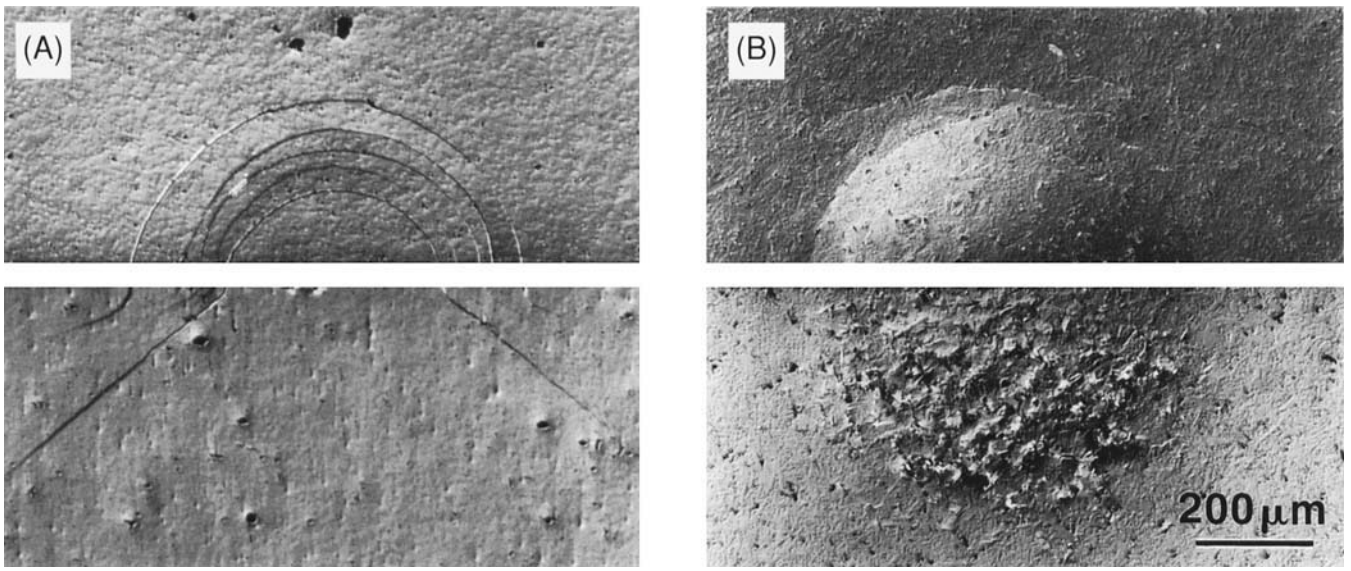

Fig. 5. Half-surface (upper) and section (lower) views of Hertzian contact damage in SiC, using tungsten carbide sphere of radius $r = 3.18$ mm at load $P = 2000$ N: (A) homogeneous fine-grain form, showing cone crack (pressure $p_0 = 7.44$ GPa); (B) heterogeneous coarse-grain form, showing distributed subsurface damage (pressure $p_0 = 7.20$ GPa). Optical Nomarski interference illumination.

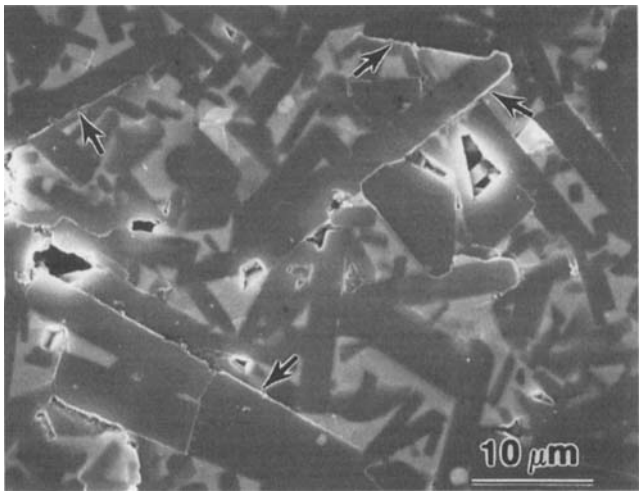

Fig. 6. SEM view of deformed area in section view of Fig. 5(B). Note debonding failures at weak interfaces.

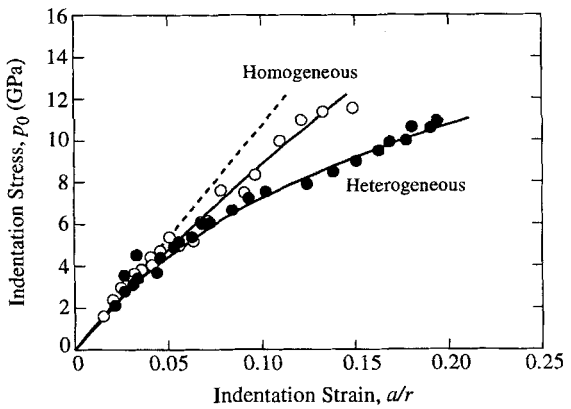

Fig. 7. Hertzian indentation stress–strain curves for SiC ceramics, in homogeneous and heterogeneous forms. Data taken with tungsten carbide spheres in the radius range $r = 1.58$ to 12.7 mm. Dashed line is Hertzian prediction Eq. (3) for elastic contact.

IV. Discussion

We have demonstrated in our study on SiC that one can induce significant changes in the toughness response of ceramics by suitably enhancing the microstructural heterogeneity. Micrographically, our tailored heterogeneous SiC material shows an enhanced fracture resistance from crack-wake bridging at elongated grains (Fig. 2); at the same time, the material becomes highly susceptible to local debonding failures at interphase boundaries (Fig. 6). The controlling microstructural factors in this context are grain coarsening and elongation, weakening of grain and interphase boundaries, and introduction of high internal residual stress.[29]

These observations are quantitatively validated by the indentation–strength data (Fig. 3). The heterogeneous material exhibits significant flaw tolerance, relative to the classical $\sigma_F \propto P^{-1/3}$ data set for the homogeneous control material. This tolerance corresponds to a significantly rising toughness curve $T(c)$ (Fig. 4(B)), relative to the estimated single-valued toughness $T = T_0 = 2.1$ MPa·m$^{1/2}$ for the control (Fig. 4(A)). Note that whereas $T(c)$ rises above $T = T_0$ at $c > 100$ μm ("shielding" region), it extrapolates below $T = T_0$ at $c < 100$ μm ("anti-shielding" region), suggesting a degradation of toughness at the microstructural level.[29] Again, the modifications to the SiC microstructure involve a trade-off between long-crack and short-crack properties.

Previous studies on alumina ceramics demonstrate that trade-offs of this kind have profound implications concerning microstructural design. On the one hand, increased long-crack toughness improves flaw tolerance and thereby makes ceramic components less susceptible to strength loss from spurious damage during service.[36] On the other, decreased short-crack toughness diminishes resistance to abrasive wear[18] and contact fatigue.[24] An extended study on our SiC material is currently under way to quantify the contact fatigue.[37,38] At the same time, the diminished short-crack properties have some potential benefits, by imparting a certain quasi ductility to the intrinsic mechanical response.[39] Such "ductility" is evident as the bend-over in the indentation stress–strain curve for the heterogeneous SiC in Fig. 7 and is attributable to the shear-fault-driven interface debonding damage zone that evolves in the contact subsurface in place of the well-defined, tensile-driven cone crack that typifies the traditional homogeneous brittle solid.[24,25] In this way, the load-bearing and energy-absorbing capacities of brittle

ceramics may be substantially enhanced by appropriate microstructural design.

Acknowledgments: We thank Hongda Cai and Fernando Guiberteau for discussions on parts of this work.

References

[1]N. P. Padture, "*In Situ*-Toughened Silicon Carbide," *J. Am. Ceram. Soc.*, **77** [2] 519–23 (1994).

[2]R. Steinbrech, R. Knehans, and W. Schaarwächter, "Increase of Crack Resistance during Slow Crack Growth in Al_2O_3 Bend Specimens," *J. Mater. Sci.*, **18** [10] 265–70 (1983).

[3]P. L. Swanson, C. J. Fairbanks, B. R. Lawn, Y.-W. Mai, and B. J. Hockey, "Crack-Interface Grain Bridging as a Fracture Resistance Mechanism in Ceramics: I, Experimental Study on Alumina," *J. Am. Ceram. Soc.*, **70** [4] 279–89 (1987).

[4]P. L. Swanson, "Crack-Interface Traction: A Fracture-Resistance Mechanism in Brittle Polycrystals," pp. 135–55 in Advances in Ceramics, Vol. 22, *Fractography of Glasses and Ceramics*. Edited by J. Varner and V. D. Frechette. American Ceramic Society, Columbus, OH, 1988.

[5]Y.-W. Mai and B. R. Lawn, "Crack-Interface Grain Bridging as a Fracture Resistance Mechanism in Ceramics: II, Theoretical Fracture Mechanics Model," *J. Am. Ceram. Soc.*, **70** [4] 289–94 (1987).

[6]S. J. Bennison and B. R. Lawn, "Role of Interfacial Grain-Bridging Sliding Friction in the Crack-Resistance and Strength Properties of Nontransforming Ceramics," *Acta Metall.*, **37** [10] 2659–71 (1989).

[7]R. F. Cook, "Segregation Effects in the Fracture of Brittle Materials: Ca–Al_2O_3," *Acta Metall.*, **38** (6) 1083–100 (1990).

[8]R. W. Steinbrech, A. Reichl, and W. Schaarwächter, "*R*-Curve Behavior of Long Cracks in Alumina," *J. Am. Ceram. Soc.*, **73** [7] 2009–15 (1990).

[9]B. R. Lawn, N. P. Padture, L. M. Braun, and S. J. Bennison, "Model for Toughness-Curves in Two-Phase Ceramics: I, Basic Fracture Mechanics," *J. Am. Ceram. Soc.*, **76** [9] 2235–40 (1993).

[10]N. P. Padture, J. L. Runyan, S. J. Bennison, L. M. Braun, and B. R. Lawn, "Model for Toughness-Curves in Two-Phase Ceramics: II, Microstructural Variables," *J. Am. Ceram. Soc.*, **76** [9] 2241–47 (1993).

[11]G. H. Beall, "Structure, Properties, and Applications of Glass-Ceramics"; pp. 251–61 in *Advances in Nucleation and Crystallization in Glasses*. Edited by L. L. Hench and S. W. Freiman. American Ceramic Society, Columbus, OH, 1972.

[12]C. K. Chyung, G. H. Beall, and D. G. Grossman, "Microstructures & Mechanical Properties of Mica Glass-Ceramics"; pp. 1167–94 in *Electron Microscopy and Structure of Materials*. Edited by G. Thomas, R. M. Fulrath, and R. M. Fisher. University of California Press, Berkeley, CA, 1972.

[13]C.-W. Li and J. Yamanis, "Super-Tough Silicon Nitride with *R*-Curve Behavior," *Ceram. Eng. Sci. Proc.*, **10** [7–8] 632–45 (1989).

[14]C.-W. Li, D.-J. Lee, and S.-C. Lui, "*R*-Curve Behavior and Strength of *in-Situ* Reinforced Silicon Nitride with Different Microstructures," *J. Am. Ceram. Soc.*, **75** [7] 1777–85 (1992).

[15]P. F. Becher, "Microstructural Design of Toughened Ceramics," *J. Am. Ceram. Soc.*, **74** [2] 255–69 (1991).

[16]N. P. Padture, "Crack Resistance and Strength Properties of Some Alumina-Based Ceramics"; Ph.D. Dissertation. Lehigh University, Bethlehem, PA, 1991.

[17]P. Chantikul, S. J. Bennison, and B. R. Lawn, "Role of Grain Size in the Strength and *R*-Curve Properties of Alumina," *J. Am. Ceram. Soc.*, **73** [8] 2419–27 (1990).

[18]S.-J. Cho, B. J. Hockey, B. R. Lawn, and S. J. Bennison, "Grain-Size and *R*-Curve Effects in the Abrasive Wear of Alumina," *J. Am. Ceram. Soc.*, **72** [7] 1249–52 (1989).

[19]S.-J. Cho, H. Moon, B. J. Hockey, and S. M. Hsu, "The Transition from Mild to Severe Wear in Alumina during Sliding," *Acta Metall.*, **40** [1] 185–92 (1992).

[20]R. F. Cook, B. R. Lawn, and C. J. Fairbanks, "Microstructure-Strength Properties in Ceramics: I, Effect of Crack Size on Toughness," *J. Am. Ceram. Soc.*, **68** [11] 604–15 (1985).

[21]R. F. Cook, C. J. Fairbanks, B. R. Lawn, and Y.-W. Mai, "Crack Resistance by Interfacial Bridging: Its Role in Determining Strength Characteristics," *J. Mater. Res.*, **2** [3] 345–56 (1987).

[22]L. M. Braun, S. J. Bennison, and B. R. Lawn, "Objective Evaluation of Short-Crack Toughness-Curves Using Indentation Flaws: Case Study on Alumina-Based Ceramics," *J. Am. Ceram. Soc.*, **75** [11] 3049–57 (1992).

[23]D. B. Marshall, "An Improved Biaxial Flexure Test for Ceramics," *Am. Ceram. Soc. Bull.*, **59** [5] 551–53 (1980).

[24]F. Guiberteau, N. P. Padture, H. Cai, and B. R. Lawn, "Indentation Fatigue: A Simple Cyclic Hertzian Test for Measuring Damage Accumulation in Polycrystalline Ceramics," *Philos. Mag. A*, **68** [5] 1003–16 (1993).

[25]F. Guiberteau, N. P. Padture, and B. R. Lawn, "Effect of Grain Size on Hertzian Contact in Alumina," *J. Am. Ceram. Soc.*, **77** [7] 1825–31 (1994).

[26]R. F. Cook and D. H. Roach, "The Effect of Lateral Crack Growth on the Strength of Contact Flaws," *J. Mater. Res.*, **1** [4] 589–99 (1986).

[27]D. B. Marshall, B. R. Lawn, and P. Chantikul, "Residual Stress Effects in Sharp-Contact Cracking: II. Strength Degradation," *J. Mater. Sci.*, **14** [9] 2225–35 (1979).

[28]Y.-W. Mai and B. R. Lawn, "Crack Stability and Toughness Characteristics in Brittle Materials," *Ann. Rev. Mater. Sci.*, **16**, 415–39 (1986).

[29]B. R. Lawn, *Fracture of Brittle Solids*; 2nd ed. Cambridge University Press, Cambridge, U.K., 1993.

[30]B. R. Lawn, A. G. Evans, and D. B. Marshall, "Elastic/Plastic Indentation Damage in Ceramics: The Median/Radial Crack System," *J. Am. Ceram. Soc.*, **63** [9–10] 574–81 (1980).

[31]B. R. Lawn and T. R. Wilshaw, "Indentation Fracture: Principles and Applications," *J. Mater. Sci.*, **10** [6] 1049–81 (1975).

[32]D. Tabor, *Hardness of Metals*. Clarendon, Oxford, U.K., 1951.

[33]T. O. Mulhearn, "The Deformation of Metals by Vickers-Type Pyramidal Indenters," *J. Mech. Phys. Solids*, **7**, 85–96 (1959).

[34]K. L. Johnson, *Contact Mechanics*. Cambridge University Press, London, U.K., 1985.

[35]M. V. Swain and B. R. Lawn, "A Study of Dislocation Arrays at Spherical Indentations in LiF as a Function of Indentation Stress and Strain," *Phys. Status Solidi*, **35** [2] 909–23 (1969).

[36]S. J. Bennison, J. Rödel, S. Lathabai, P. Chantikul, and B. R. Lawn, "Microstructure, Toughening Mechanisms and Mechanical Properties of Alumina Ceramics"; pp. 209–33 in *Toughness Curves in Quasi-Brittle Materials*. Edited by S. P. Shah. Kluwer Academic Publishers, Dordrecht, The Netherlands, 1991.

[37]N. P. Padture and B. R. Lawn, "Fatigue in Ceramics with Interconnecting Weak Interfaces: a Study Using Cyclic Hertzian Contacts," *Acta Metall. Mater.*, in press.

[38]N. P. Padture and B. R. Lawn, "Contact Fatigue of a Silicon Carbide with a Heterogeneous Grain Structure," *J. Am. Ceram. Soc.*, in press.

[39]B. R. Lawn, N. P. Padture, H. Cai, and F. Guiberteau, "Making Ceramics 'Ductile'," *Science (Washington, D.C.)*, **263**, 1114–16 (1994). □